

AperTO - Archivio Istituzionale Open Access dell'Università di Torino

Designing rGO/MoS₂ hybrid nanostructures for photocatalytic applications

This is the author's manuscript

Original Citation:

Availability:

This version is available <http://hdl.handle.net/2318/1607705> since 2016-10-26T12:21:40Z

Published version:

DOI:10.1039/c6ra08633k

Terms of use:

Open Access

Anyone can freely access the full text of works made available as "Open Access". Works made available under a Creative Commons license can be used according to the terms and conditions of said license. Use of all other works requires consent of the right holder (author or publisher) if not exempted from copyright protection by the applicable law.

(Article begins on next page)



UNIVERSITÀ DEGLI STUDI DI TORINO

This is an author version of the contribution published on:

Questa è la versione dell'autore dell'opera:

RSC Advances

Volume 6, Issue 64, 2016, Pages 59001-59008

DOI: 10.1002/slct.201600278

The definitive version is available at:

<http://pubs.rsc.org/en/content/articlelanding/2016/ra/c6ra08633k#!divAbstract>

Designing rGO/MoS₂ hybrid nanostructures for photocatalytic applications

Sara Cravanzola, Federico Cesano, Giuliana Magnacca, Adriano Zecchina and Domenica Scarano

Graphene and its derivatives exhibit large surface area, being ideal templates to facilitate the nucleation, growth or interaction of a huge variety of structures. Among them, molybdenum disulphide, with its structural and morphological compatibility with graphene, can be a candidate for achieving an excellent integration, to make new hybrid nanocomposites with outstanding characteristics. Among the synthesis methods of graphene/MoS₂ composites, the solution-phase exfoliation of a MoS₂/graphite mixture, by means of ultrasounds, shows significant advantages in terms of large amount production without altering the main properties of 2D nanomaterials. Moreover MoS₂, having a strong absorption in the visible, has been exploited as a novel visible light-sensitive semiconductor photocatalyst. But, due to the quick recombination of photo-generated charge carriers, the photocatalytic efficiency of MoS₂ has to be further improved. Graphene and graphene related materials, as excellent electron-acceptor/transport materials, have been applied to photocatalysis, because they are able to decrease the photo-generated electron-hole recombination, thus improving the light absorption. Therefore, MoS₂ and graphite oxide (GO) have been simultaneously sonicated in an ethanol/water mixture and characterized from the structure, morphology and electronic properties point of view. The composite was thermally treated in such a way to reduce GO and the photocatalytic activity of the reduced GO/MoS₂ has been investigated by means of UV-vis spectroscopy, following the degradation of methylene-blue (MB) under solar-like irradiation.

Department of Chemistry, NIS (Nanostructured Interfaces and Surfaces) Interdepartmental Centre and INSTM Centro di Riferimento, University of Torino, Via P. Giuria, 7, 10125 Torino, Italy. E-mail: federico.cesano@unito.it

1. Introduction

The interest in mono-dimensional (1D) and layered (2D) materials has been increased in the last few years due to the fact that such materials are expected to show improved properties as compared with traditional materials. In this domain, many classes of materials have been investigated, including titanate nanotubes,^{1,2} carbon nanotubes,³ layered and layered double hydroxides like hydrotalcite,^{4,5} transition metal dichalcogenides (e.g. MoS₂, WS₂, TiS₂)^{6,7} and 2D carbon (i.e. single-layer/few-layer graphene).⁸ As far as carbon-based materials with different dimensionality are concerned, the increasing attention is due to their unique properties, ranging from electrical conductivity to biocompatibility, mechanical and thermal stability.^{9–11} Taking into consideration these aspects, compared with more traditional carbons some properties of new carbons are expected to be improved, and the prospective applications are diverse, including absorbents, catalyst carriers, electrodes and supports.^{12–14}

In particular, as for graphene and its derivatives, due to their large surface area, they are ideal templating materials to facilitate the nucleation, growth or interaction of a huge variety of structures, from organic (polymers or biomolecules) to inorganic (oxides, oxide derivatives), for the production of functional hybrid nanocomposites.⁸

New opportunities and applications can come from the union of the peculiar properties of polymers, such as resistance to chemical corrosion, simplicity of manufacturing, low density and lightweight, together with the peculiar mechanical and electrical properties of the graphene-based conducting fillers,^{15,16} thus developing nanocomposites, whose well-known piezoresistive nature¹⁷ makes them suitable for sensing applications, including pressure,¹⁸ tactile,¹⁹ flow sensors²⁰ and for monitoring the structural integrity of mechanical elements.²¹

Moreover, graphene could be beneficial in biomedical applications and electrochemical biosensing,²² being involved in different combinations with a wide range of biomolecules, from DNA, aminoacids and proteins, to cells and bacteria.^{23,24}

Concerning carbon-inorganic composites, various metallic-based nanostructures like Pt, Co, Si, Al, Mg, Cu and Al/Au, Pd/Au, Mg/Sn have been successfully anchored to graphene nano-sheets, to enhance performances ranging from catalysis to electronics and sensors.²⁵

In addition, to further improve their properties, a number of metal oxides such as TiO_2 , SiO_2 , ZnO , SnO_2 , MnO_2 , Co_3O_4 , Fe_3O_4 has been grown on graphene nanosheets via different synthetic approaches.²⁶ Notably, synergy effects between nanocarbons and TiO_2 have been shown for the photocatalytic degradation of organic pollutants compounds.^{3,27}

It is noteworthy that molybdenum disulphide, a transition metal dichalcogenide (TMD), due to its physical, optical, electrical and structural properties, can be an excellent candidate for being combined with graphene and graphene derivatives, originating new hybrid nanocomposites with outstanding characteristics.^{28–31}

The achievable applications of this kind of nanocomposite are depending on the adopted synthesis approach. In the bottom up approach, graphene-based structures are mixed with an aqueous solution of a MoS_2 precursor, e.g. ammonium tetrathiomolybdate,³² or with a mix of ammonium eptamolybdenate or sodium molybdate dihydrate³³ and thiourea,³⁴ thus obtaining a nanocomposite, which can be suitable as counter-electrode in dye-sensitized solar cells. The ion intercalation technique represents another possible way to synthesize layered MoS_2 /graphite composites, thus making them suitable for lithium-ion batteries.³⁵ On the other hand, the top-down approach, consisting in breaking up the massive and bulk MoS_2 material, allows to obtain particles of decreased dimensions. In particular, the solution-phase exfoliation of a MoS_2 /graphite mixture, by means of ultrasounds, shows significant advantages in terms of large amount production without altering the molecular structures and the intrinsic electronic properties of 2D nanomaterials.³⁶

Beside all the promising applications of MoS_2 /graphite composites, it is important to underline that mono-layers and few-layers of MoS_2 , obtained from liquid exfoliation, suffer seriously from the restacking phenomena,³⁷ which would directly suppress the charming advantages of 2D MoS_2 . This problem can be satisfactorily solved by introducing graphene as a sort of intercalating compound, which can avoid the complete restacking of MoS_2 layer, as shown in literature for a system composed by MoS_2 and WS_2 .³⁸ Moreover, MoS_2 has a strong absorption in the visible spectrum region, therefore it has been exploited as a novel visible light-sensitive semiconductor photocatalyst for photocatalytic applications.^{39,40} However, due to the quick recombination of photo-generated charge carriers,⁴¹ the photocatalytic efficiency of MoS_2 has to be further improved. Along this line, graphene and graphene derivatives, as excellent electron-acceptor/transport materials, have been applied to photocatalysis, because they are able to decrease the photo-generated electron–hole recombination, thus improving the light absorption.^{42,43} The structural and morphological compatibility between graphene-like materials and single-layer MoS_2 sheets should enable better intercalation to achieve the anticipated benefits of such integration.

Following this line, it would be of great interest to analyze the results of the simultaneous solvent-assisted ultrasonication of graphite and molybdenum disulphide.

As far as the choice of the sonication solvent is concerned, it is well known that the effectiveness of the exfoliation process of

nanomaterials in liquids can be partially predicted by the theory of Hansen solubility parameters.^{44–46} In this domain, it has been shown⁴⁷ that the use of alcohols, although generally considered “poor” solvents (low specific Hansen solubility) makes it possible to exfoliate and to fragment thick MoS_2 flakes into thin sheets and small particles.

The features of the sonicated samples could give answers to unsolved questions, concerning: (i) the peculiar effects of sonication on both graphite and MoS_2 ; (ii) the most appropriate solvent to be used; (iii) the enhanced properties of the obtained composite when compared to the single components; (iv) the morphology of the resulting composite material, and interactions established between graphite, molybdenum disulphide and solvent; (v) the effectiveness of the sonication in obtaining a composite with a structure characterized by intercalation of alternate MoS_2 and graphene layers. Recent investigations have shown that stacked MoS_2 /graphene hybrids can be obtained⁴⁸ and that the interlayer coupling, electric shields, and interface/contact regions may affect the electronic structure making these heterobilayers suitable for nanoelectronic devices.^{49,50} Among these property enhancements, recent computing and calculations have allowed the understanding about the best structure able to optimize interactions in layered materials.⁵¹

Taking into consideration these property enhancements, the coupling between graphite oxide (GO) and MoS_2 slabs for photocatalysis has been investigated in this paper. In this domain, GO and MoS_2 have been simultaneously sonicated in an ethanol/water mixture, for the first time. Notice that GO was used as a starting carbon-based material because of its high oxygen-based functionalization, that could help the establishment of interactions with MoS_2 and, then, makes its surface hydrophilic. This allows therefore a more easy dispersion in a water-based solvent. The obtained composite materials have been characterized by means of scanning electron microscopy (SEM), energy dispersive X-rays (EDAX), X-ray diffraction (XRD). The GO/ MoS_2 composites have also been thermally reduced, in such a way to obtain reduced GO/ MoS_2 composite (rGO/ MoS_2). However, the thermal reduction of GO is a very complex process because of the multistep thermal removal of intercalated H_2O molecules and oxide groups coming from carboxyl, hydroxyl and epoxy groups.⁵² The obtained rGO/ MoS_2 has been also characterized. The catalytic activity of the rGO/ MoS_2 has been investigated using UV-vis spectroscopy, following the degradation of methylene-blue (MB) under solar-like irradiation.

2. Experimental

2.1 Materials and synthesis

2.1.1 Graphite oxide. Graphite oxide was synthesized from graphite powder, following the modified Hummer's method. More in detail, 46 ml of H_2SO_4 (98%) were slowly added to 1 g graphite powder in a 500 ml flask, put into an ice bath, to avoid a sudden increase of temperature, and left under stirring for 1 hour. Then, KMnO_4 (6 g) was inserted gradually into the flask and, after 1 hour-stirring, temperature was raised to 35 °C for 12 hours. After that, H_2O (40 ml) was added and temperature increased to 90 °C for 15 minutes. After cooling down the

temperature to RT, other H₂O (200 ml) was added to the sample, lev stirring for 1 hour and H₂O₂ (6 ml, 30%) was added and lev stirring at RT for 48 hours. Finally, the so-obtained GO was washed with HCl (5%) for 5 times and then with H₂O for other 5 times, then centrifuged at 10 000 rpm (relative centrifugal force, RCF $\frac{1}{4}$ 10 397 \times g) for 10 minutes.

2.1.2 GO/MoS₂ composite. GO/MoS₂ composite was obtained by dispersing the as-prepared GO and MoS₂ powder (Fluka), 1 : 1 weight ratio, in 10 ml 45 vol% ethanol/water mixture (EtOH/H₂O). Such volume fraction of ethanol in water has been established on the basis of literature data.⁵³ In fact, it has been shown that the concentrations of graphene and inorganic graphene analogues dispersions are strongly dependent on the volume fraction of ethanol in water.⁵³

The dispersion was sonicated at 20 kHz for 6 hours by a VCX 500 Sonics Vibracell ultrasonic processor (power 500 W) equipped with a Ti alloy tapered microtip (d $\frac{1}{4}$ 3 mm, 30% amplitude). In order to control the temperature and to avoid the evaporation of the solvent, the dispersion was put into an ice bath during the whole sonication step. The obtained dark solution was lev overnight at RT to allow the evaporation of EtOH/H₂O and the obtained dark powder was then collected to be analysed.

2.1.3 rGO/MoS₂ composite. The thermal reduction of the GO/MoS₂ composite to rGO/MoS₂ was carried out by means of a thermal gravimetric analyzer (TGA, TA Instruments, Q600) under controlled N₂ atmosphere and controlled temperature (5 °C min⁻¹ ramp to 400 °C and isotherm for 60 minutes).

2.2 Methods

Morphology and structure of the samples have been investigated by means of scanning electron microscope (SEM) Zeiss Evo50. The morphology has been obtained by means of secondary electrons. More detailed information has been obtained by high resolution transmission electron microscopy (HRTEM) with a JEOL 3010-UHR instrument operating at 300 kV, equipped with a 2k \times 2k pixels Gatan US1000 CCD camera.

X-ray diffraction (XRD) patterns on MoS₂, graphene oxide, GO/MoS₂ composite and rGO/MoS₂ composite have been collected with a diffractometer (PANalytical PW3050/60 X'Pert PRO MPD) by using a Ni-filtered Cu anode and working with re ϕ ectance Bragg–Brentano geometry.

UV-visible spectra have been acquired in the transmission mode at room temperature by using a double-beam UV-vis-NIR spectrophotometer (Varian Cary UV 5000) operating in the wavelength range of 190–1000 nm.

The choice of the reduction temperature for GO/MoS₂ composite was made by examining the weight loss vs. temperature curve, as obtained by thermal gravimetric analysis (TGA, TA Instruments, Q600), in N₂ atmosphere (Fig. S1, ESI†). It is observed that, starting from 200 °C, a rapid 20% mass loss, due to the removal of the oxygen-containing functional groups,⁵⁴ in the form of CO, CO₂ and steam, has occurred.⁵⁵

Diffuse re ϕ ectance infrared Fourier transform spectroscopy (DRIFT) has been adopted to investigate the presence of functional groups (i.e. oxygen-containing species) on the different

samples. Each sample was preventively dried in air at 100 °C. FTIR spectra were collected in air by using 128 scans and a resolution of 4 cm⁻¹, with a Nicolet 6700 spectrophotometer equipped with a DRIFT Smart Accessory and a MCT detector. The re ϕ ectance spectra were converted in Kubelka–Munk units.

2.2.1 Photodegradation test. 6.5 mg rGO/MoS₂ and other powder samples, used as reference (6.5 mg MoS₂ and 6.5 mg P25 TiO₂), were dispersed in separated aliquots (8.5 ml) of a methylene blue (MB) water solution (12.5 mg L⁻¹). Samples were kept in the dark at RT for 1 hour. After exposure to a solar lamp, the sample dispersions were centrifuged at 10 000 rpm for 30 min. Photocatalytic degradation of MB has been investigated using UV-vis spectroscopy in the transmission mode. The solar light simulating irradiation was carried out at 25 °C \pm 5 using a SOL2/500S lamp (Honle UV technology, Munchen, Germany). The SOL-bulb and the H₂ filter together yield a spectrum, which is very similar to the natural sunlight, ranging from ultraviolet to infrared radiation (295–3000 nm). The integrated intensity of the adsorbed MB manifestations (C) was used to obtain C/C₀ vs. time plots, where C₀ is the concentration, corresponding to the initial intensity before illumination.

3. Results and discussion

3.1 Structure and morphology of GO/MoS₂ and rGO/MoS₂

XRD measurements have been performed to investigate the effects of the sonication and of the thermal treatment on the structures of the composite materials. Fig. 1 shows the patterns of bulk GO and bulk MoS₂ as compared to GO/MoS₂ composite after sonication and rGO/MoS₂ composite after the thermal treatment at 400 °C.

More in detail, bulk GO (grey pattern, a) shows a main peak at 2 θ \approx 10.5° (d-spacing of 0.84 nm), which indicates that GO retains a layered character without a strict crystalline lattice. As well-known, the d-spacing of GO planes along the c-axis is higher if compared to that of a typical graphite (3.35 Å, due to the presence of oxygen-based functional groups between planes. Besides, bulk MoS₂ (black pattern, b) reveals its typical crystalline nature, with narrow peaks, the more intense of which at 2 θ \approx 14.5° is due to the (002) diffraction planes, which corresponds to a d \approx 6.15 Å (PDF card #037-1492).

Moving to GO/MoS₂ composite (red pattern, c), the main diffraction peaks of MoS₂ are also observed, whereas a broad feature due to GO is appearing (marked with the asterisk). From this, we conclude that, during the sonication process, the MoS₂ crystalline structure is maintained, while GO particles undergo a strong fragmentation, which gives rise to small and amorphous particles, as a result of the superior effectiveness of the sonication on GO rather than on MoS₂. From the Scherrer's equation ($L \approx K\lambda/b \cos \theta$, where: λ is the X-ray wavelength, b is the FWHM of the diffraction line corrected by the instrumental broadening, θ is the diffraction angle, and K is a shape constant, which has been assumed to be 0.76), the mean crystallite thickness of the MoS₂ particles was calculated (for bulk MoS₂ and for GO/MoS₂). More in details, from the 2 θ \approx 14.5° XRD peak, assigned to the (002) MoS₂ crystalline planes,

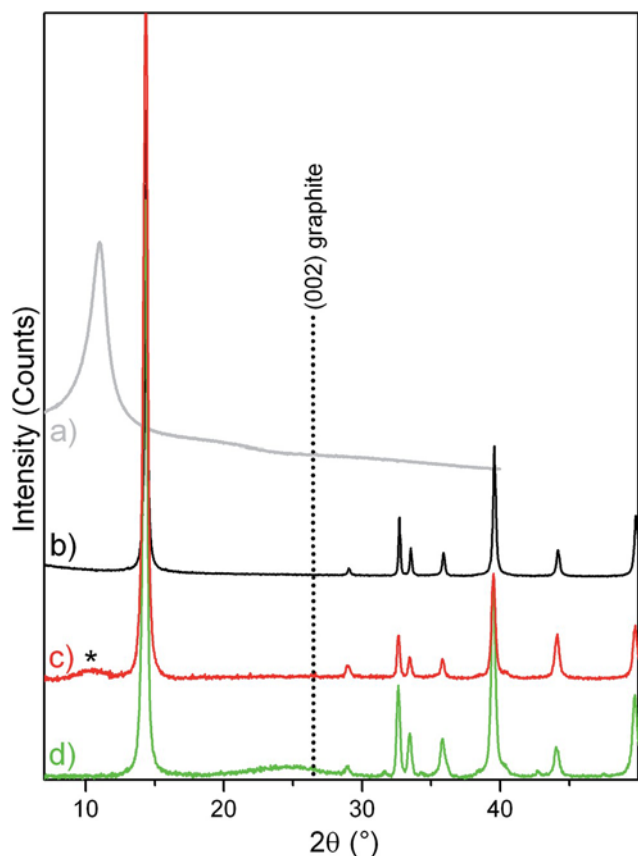


Fig. 1 XRD patterns of: (a) bulk GO, grey line; (b) bulk MoS₂, black line; (c) GO/MoS₂ composite after sonication, red line; (d) rGO/MoS₂ composite after thermal treatment, green line. The asterisk of pattern (c) corresponds to the peak position of GO, while the (002) XRD line position of the graphite (PDF card #41-1487) is reported for comparison.

nanocrystals about 60 nm (99 layers) in thickness are obtained for bulk MoS₂, while nanocrystals of about 18 nm (30 layers) are evaluated for GO/MoS₂ after sonication. From this, a moderate

effect of the sonication step on the size reduction of MoS₂ is evidenced.

Finally, moving to rGO/MoS₂ composite (green pattern, d), the GO feature is totally absent, while a small new feature is arising at $2\theta \approx 24.4^\circ$, corresponding to a d-spacing between the graphene planes of about 3.6 Å which is closer to the position of (002) diffraction planes of hexagonal graphite ($d \approx 3.35$ Å). Besides the peak position, which is indicative of the crystal structure and symmetry of the contributing phase(s), a low crystallinity (i.e. high-defective character) of the rGO phase, can be highlighted from the FWHM (full-width-at-half-maximum) of the XRD band at $2\theta \approx 24.4^\circ$.⁵⁶ From this, we can hypothesize only a partial restoration of the graphitic phase, as a consequence of the thermal treatment at 400 °C. It is worth noticing that the thermal treatment leads to an increase of the MoS₂ particle thickness, up to about 34 nm (57 layers), as calculated by applying the Scherrer's equation.

The GO/MoS₂ composite, as obtained after sonication in EtOH/H₂O and evaporation of the solvent is SEM imaged in Fig. 2a and b. From these, a quite complex morphology of the composite is obtained, with aggregates of differently oriented platelets, having a heterogeneous distribution of sizes, ranging from some μm to a few nanometers. Nevertheless, the layered structure of the sample, made by the packing of bidimensional MoS₂ and GO sheets can be highlighted.

More detailed information is obtained from the HRTEM images shown in Fig. 2c and d.

The in-focus image of a portion of GO/MoS₂ composite reveals the presence of highly crystalline particles, whose interference fringes, highlighted by white lines, 6.1 Å and 2.7 Å spaced, are unequivocally associated with MoS₂ (002) and (1-10) planes, respectively (Fig. 2c, left panel). Contextually, the same region of the sample is under-focus imaged (Fig. 2c, right panel), allowing to distinguish the amorphous portion of the composite, whose edge regions highlighted by white arrows, embed the MoS₂ particle. Therefore, the non-crystalline area can be identified with GO decorating and covering the MoS₂

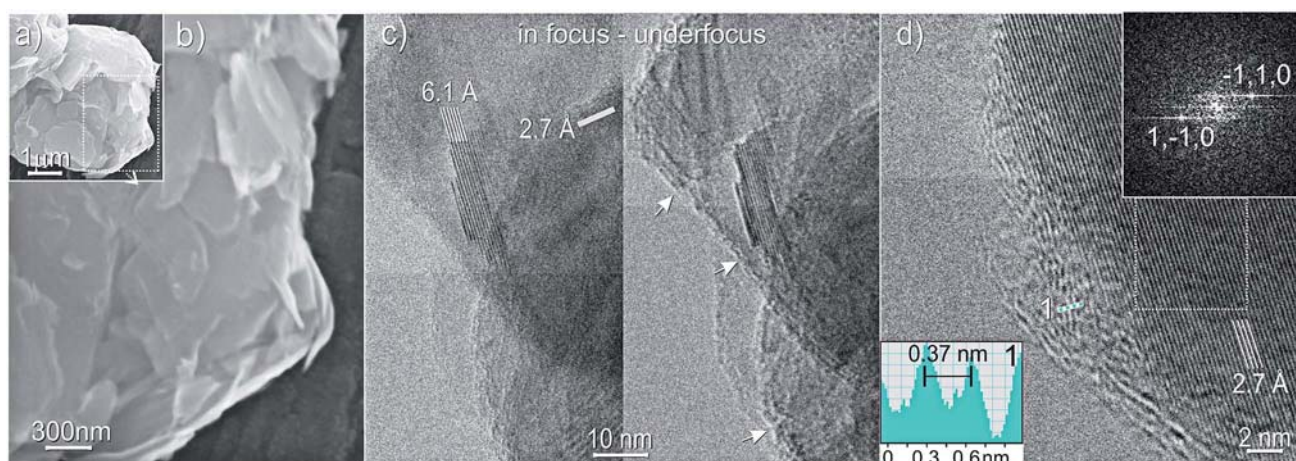


Fig. 2 (a) SEM image and (b) enlarged view of GO/MoS₂ composite; (c) in-focus (left panel) and under-focus (right panel) HRTEM images of a portion of GO/MoS₂ composite; (d) HRTEM image of rGO/MoS₂ composite as obtained after the thermal treatment at 400 °C, that is FFT imaged in the inset therein. Atomic spacing along the 1 selected direction is shown in the bottom left inset.

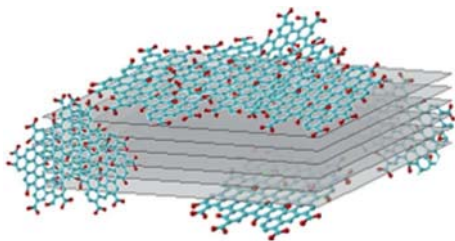


Fig. 3 Proposed model for GO/MoS₂ and rGO/MoS₂ composites.

surface, as confirmed by the before discussed XRD patterns, from which the amorphous nature of GO particles, due to strong sonication effects, has been shown.

Besides, rGO/MoS₂ composite, as obtained after the thermal treatment at 400 °C, is HRTEM imaged in Fig. 2d, where white lines highlight lattice fringes 2.7 Å spaced, associated with (1-10) planes of few-layer thick crystalline MoS₂. The MoS₂ structure is confirmed by the corresponding fast-Fourier-transform (FFT) imaged in the inset at the top of Fig. 2d, which shows bright spots associated with {1-10} plane families. In the partially amorphous border region, interference fringes (white and light blue dots) 3.7 Å spaced, as shown in the inset at the bottom of the figure, are arising, due to the building up of graphitic phases, are observed in agreement with XRD investigations.

A model of the arrangement of GO and of rGO on MoS₂ slabs is shown in Fig. 3, which summarizes the previously discussed HRTEM results.

3.2 Optical and surface properties

The optical properties of the samples just after the sonication were evaluated by UV-vis spectroscopy. The spectra of MoS₂ (black line), GO (grey line), GO/MoS₂ (red line) sonicated in EtOH/H₂O and rGO/MoS₂ (green line) redispersed in EtOH/H₂O are compared in Fig. 4a.

MoS₂ shows the A, B, C and D typical excitonic peaks (15 000 cm⁻¹, 16 500 cm⁻¹, 22 300 cm⁻¹ and 25 100 cm⁻¹ respectively), whose nature is well described in literature.⁴⁷ Furthermore, GO presents a first band at about 43 860 cm⁻¹ attributed to $\pi \rightarrow \pi^*$ transitions of C=C and a second one at about 32 680 cm⁻¹ attributed to $n \rightarrow \pi^*$ transitions of C=O.⁵⁷ Moving to the spectrum of GO/MoS₂ composite (red line), all the typical features described for MoS₂ and GO are observed, while rGO/MoS₂ is highly absorbing in the whole 45 000–10 000 range as expected for a system characterized by extended C=C sp^2 domains.⁵⁸ It is noteworthy that the GO bands are absent, meaning that the thermal treatment leads to the loss of functional groups containing oxygen and to the partial restoration of the sp^2 conjugation. Some more the spectrum of rGO/MoS₂ does not show clearly the typical MoS₂ C and D excitonic bands (at 22 300 cm⁻¹ and 25 100 cm⁻¹ respectively) superimposed to graphene background. This fact is likely associated with photoluminescence effects that have been reported for MoS₂ in monolayer and multilayer forms.^{41,59–63} The MoS₂ A and B excitonic bands at 15 000 cm⁻¹

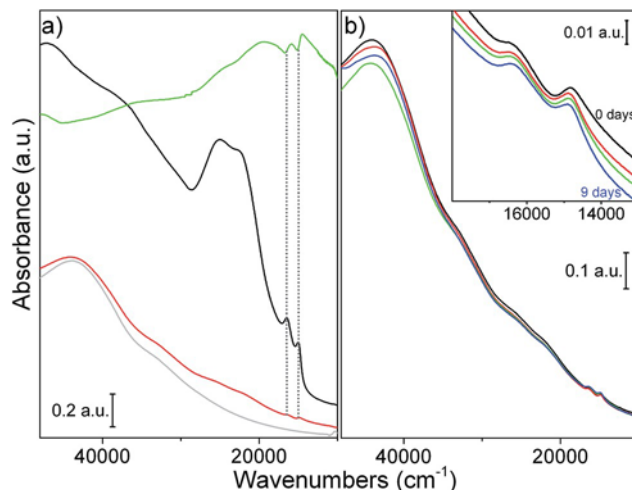


Fig. 4 UV-vis spectra of: (a) MoS₂ (black line), GO (grey line), GO/MoS₂ sonicated in EtOH/H₂O (red line) and rGO/MoS₂ redispersed in EtOH/H₂O (green line); (b) GO/MoS₂ sonicated in EtOH/H₂O acquired from 0 (black line) to 9 days after sonication; (enlarged view in the inset).

and 16 500 cm⁻¹ respectively appear to be “overturned” on rGO/MoS₂ when compared to MoS₂ and GO/MoS₂. Specifically, a maximum of a peak of MoS₂ (black line) corresponds exactly to a minimum of the same peak of rGO/MoS₂ (green line). Although a detailed and deep study of this phenomenon is beyond the aim of this work, we hypothesize that the inversion of the shape of the bands can be due to specular reflectance effects, becoming important for a very highly absorbing material made by poorly dispersed particles with large dimensions.⁶⁴ That insufficient dispersion can be also inferred from the consideration that rGO/MoS₂ derives from GO/MoS₂ that was subjected to: removal of the solvent after sonication, thermal reduction treatment and finally redispersion in solvent for UV-vis measurements. The whole procedure plausibly undoes the effects of dispersion and exfoliation obtained during sonication.

Some more, to evaluate the stability of GO/MoS₂ dispersion in EtOH/H₂O, UV-vis spectra of the composite, just sonicated and then after 2, 4 and 9 days, were acquired. The obtained results are shown in Fig. 4b. In this figure and in the inset therein, no significant shift and intensity decrease of A and B excitonic peaks are observed. As reported by some authors, the position of the A and B bands is affected by the particles sizes due to a quantum size effect.^{47,65} Then, we can state that for our samples no restacking or strong precipitation and deposition phenomena are occurring through time, being the particles durably well dispersed in the solvent. This result is in agreement with the fact that the 45% vol EtOH/H₂O mixture has resulted to be efficient in obtaining a good dispersion degree of particles, according to its Hansen solubility parameters.⁵³

DRIFT spectroscopy has been adopted to investigate the presence of functional groups (i.e. oxygen species) on the different sample surfaces. DRIFT spectra of GO (grey line), GO/MoS₂ (red line), and of rGO/MoS₂ (green line) are compared

with the spectrum of the bulk native MoS₂ (black line) in the 3900–1300 cm⁻¹ region (Fig. 5). Several common fingerprints for GO and GO/MoS₂ can be highlighted. In particular, the wide absorption in the 3700–2500 cm⁻¹ interval is associated with n(OH) of alcoholic/phenolic and of carboxylic vibrational modes, while the absorption bands at 1800–1700 cm⁻¹ and at 1640–1590 cm⁻¹ are assigned to n(C=O) and at n(C=C) stretching modes. It is noteworthy that the intensity of the conjugated C-sp² bonds belonging to graphitic islands, would be enhanced by the presence of oxygen atoms (i.e. increase of the dipole moment).⁶⁶ As the intensity of n(C=O) and of n(C=C) vibrational modes is nearly vanishing for the rGO/MoS₂ sample, it is concluded that the quantity of the polar oxygen groups is drastically reduced upon the thermal treatment as reported in literature.^{55,67} It is concluded that DRIFT spectroscopy provides a valuable and sensitive tool to gain information on the population of the polar groups on carbon and carbon hybrids and on its substantial decrement upon reductive treatment.

3.3 Photodegradation test

Photodegradation experiments were performed by measuring the decrement of the MB concentration adsorbed on the rGO/MoS₂ composite and on a MoS₂ sample in water solutions containing the same quantity of photocatalyst, upon light

exposure for increasing time (Fig. 5). rGO/MoS₂ composite was selected to perform the photocatalytic tests as rGO is considered a semimetallic support which allows conduction, thus providing a channel for electron transport.⁶⁸

By starting from an initial dye concentration of 12.5 mg L⁻¹, the MB band evolution of the rGO/MoS₂ composite, as a function of the exposure time under visible light, is shown in Fig. 6a.

In this figure it is shown that the intensity of the two main MB bands at 15 100 cm⁻¹ and at 16 450 cm⁻¹, which are assigned to monomeric and aggregated species,^{69,70} is decreasing with the exposure time. A series of experiments has been also conducted by using different initial concentration of MB (12.5 mg L⁻¹, 6.25 mg L⁻¹ and 3.2 mg L⁻¹) on rGO/MoS₂ composite (Fig. S2, ESI†), thus showing that depending on the concentration, MB in solution may show a distinct tendency to form agglomerates, made by monomeric and polymeric species, in thermodynamic equilibrium.⁷¹ In Fig. 6b the MB photodegradation performances of the rGO/MoS₂ composite are compared to those of MoS₂, of rGO and of the well-known P25 TiO₂ photocatalyst, used as reference materials. It has been calculated that after 5 h under solar-light irradiation, the residual amount of the initial dye was about 4% for rGO/MoS₂, which is close to 1.2% P25 performance, as compared to the bare rGO and MoS₂ (10% and 20%, respectively). Although the activity of P25 TiO₂ is definitely higher than that of composite, rGO/MoS₂ composite shows a strong increment in the MB photodegradation, if compared to pure MoS₂ and pure rGO.

As for the explanation of such an improvement, two points could be highlighted: the p-p conjugation between MB and aromatic regions of graphene domains and the step-wise structure of energy levels constructed in the MoS₂/graphene composite (Fig. 7).⁷² The same considerations can be done in

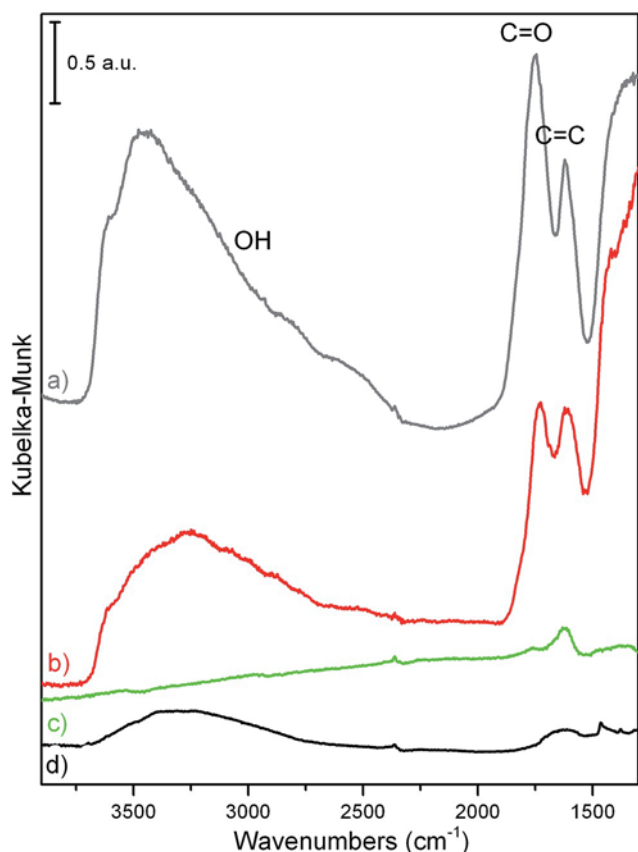


Fig. 5 DRIFT spectra of: (a) GO (grey line), (b) GO/MoS₂ sonicated in EtOH/H₂O (red line), (c) rGO/MoS₂ obtained at 400 °C (green line), and of (d) bulk MoS₂ (black line).

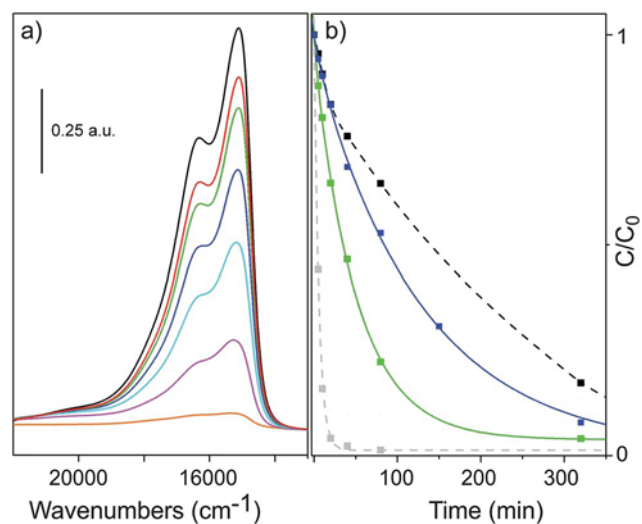


Fig. 6 (a) Evolution of the UV-vis spectra of MB (water solution) adsorbed on rGO/MoS₂ composites as a function of the exposure time under visible light (0, 5, 10, 20, 40, 80 and 320 min); (b) time dependence upon light exposure of MB adsorbed on MoS₂ (black dotted line) as compared to MB adsorbed on bare rGO, (blue line) on rGO/MoS₂ composite (green line) and on P25 TiO₂, used as a reference material (grey dotted line).

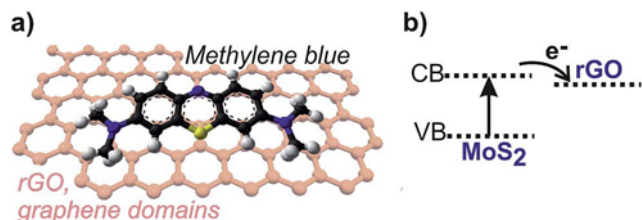


Fig. 7 (a) p–p conjugation between MB and aromatic regions of rGO and (b) the rGO acting as electron acceptor/transport, which can reduce the photogenerated electron–hole recombination and improve the light adsorption of MoS₂.

the case of the degradation of other organic dyes, due to their structure affinity with MB.

According to the data reported in literature on the conduction band, the valence band of MoS₂ (ref. 39) and the work function of graphene,⁷³ the energy levels are beneficial to transfer photo-induced electrons from the MoS₂ conduction band to the graphene, which could efficiently separate the photo-induced electrons and hinder the charge recombination in the electron-transfer processes.⁷⁴ In conclusion, rGO/MoS₂ composites have higher photocatalytic performance due to: (i) facilitated electron transfer and separation; (ii) enhancement of the light absorption intensity as consequence of the introduction of rGO; (iii) increase of the adsorption of pollutants.⁷⁴

4. Conclusions

A GO/MoS₂ composite was obtained by means of simultaneous sonication of bulk MoS₂ and GO. After the solvent evaporation, the obtained product was thermally treated and the reduction of GO/MoS₂ to rGO/MoS₂ was achieved. SEM images reveal the complex and heterogeneous morphology of the composite, while detailed information on the structures were obtained by means of HRTEM and XRD. From these, it is safely concluded that although a certain degree of exfoliation of MoS₂ particles was obtained, the sonication step is affecting more deeply the morphology and the structure of GO rather than those of MoS₂. This causes the formation of a composite made by GO small and amorphous particles decorating the surface of the more extended crystalline MoS₂ platelets. Some more, it is noteworthy that the thermal treatment at 400 °C of GO/MoS₂ leads to the restoration of the crystalline graphitic structure, with the formation of rGO/MoS₂ composite.

Finally, it has been shown the enhanced photocatalytic activity toward the photodegradation of methylene blue of rGO/MoS₂, as compared to pure MoS₂, which exhibits a quick recombination of photo-generated charge carriers.

This has been explained with the remarkable role of rGO, an excellent electron acceptor/transport material, in separating the photo-induced electrons and in hindering the charge recombination during the electron transfer process, thus enhancing the photocatalytic performances.

Acknowledgements

This work was supported by MIUR (Ministero dell'Istruzione, dell'Università e della Ricerca), INSTM Consorzio, and NIS (Nanostructured Interfaces and Surfaces) Interdepartmental Centre of University of Torino. The authors thank Dr E. Groppo her precious support in DRIFT measurements.

Notes and references

- 1 F. Cesano, S. Bertarione, M. J. Uddin, et al., *J. Phys. Chem. C*, 2010, **114**, 169–178.
- 2 S. Cravanzola, L. Muscuso, F. Cesano, et al., *Langmuir*, 2015, **31**, 5469–5478.
- 3 S. Cravanzola, S. M. Jain, F. Cesano, et al., *RSC Adv.*, 2015, **5**, 103255–103264.
- 4 C. S. Lim, Z. Sofer, O. Jankovský, et al., *RSC Adv.*, 2015, **5**, 101949–101958.
- 5 D. Scarano, S. Bertarione, F. Cesano, et al., *Surf. Sci.*, 2004, **570**, 155–166.
- 6 C. Tan and H. Zhang, *Chem. Soc. Rev.*, 2015, **44**, 2713.
- 7 H. Zhang, *ACS Nano*, 2015, **9**, 9451–9469.
- 8 D. Wu, F. Zhang, H. Liang, et al., *Chem. Soc. Rev.*, 2012, **41**, 6160–6177.
- 9 H. Dai, *Acc. Chem. Res.*, 2002, **35**, 1035.
- 10 M. S. Dresselhaus, G. Dresselhaus and P. Avouris, *Carbon Nanotubes: Synthesis, Structure, Properties, and Applications*, Springer-Verlag, New York, 2001.
- 11 C. D. Liang, Z. J. Li and S. Dai, *Angew. Chem., Int. Ed.*, 2008, **47**, 3696.
- 12 J. Chen, C. Jang, S. Xiao, et al., *Nat. Nanotechnol.*, 2008, **3**, 206.
- 13 S. Iijima, *Nature*, 1991, **354**, 56.
- 14 X. Wang, Y. Ouyang, X. Li, et al., *Phys. Rev. Lett.*, 2008, **100**, 206803.
- 15 F. Cesano, I. Rattalino, D. Demarchi, et al., *Carbon*, 2013, **61**, 63–71.
- 16 G. Haznedar, S. Cravanzola, M. Zanetti, et al., *Mater. Chem. Phys.*, 2013, **143**, 47–52.
- 17 S. Cravanzola, F. Cesano and L. Muscuso, et al., *Nanocomposites, Nanophotonics, Nanobiotechnology, and Applications*, Springer, Switzerland, 2015, p. 51.
- 18 S. Sugiyama, M. Takigawa and I. Igarashi, *Sens. Actuators*, 1983, **4**, 113–120.
- 19 B. J. Kane, M. R. Cutkosky and G. T. A. Kovacs, *J. Microelectromech. Syst.*, 2000, **9**, 425–434.
- 20 M. C. Lonergan, E. J. Severin, B. J. Brett, J. Doleman, et al., *Chem. Mater.*, 1996, **8**, 2298–2312.
- 21 S. Cravanzola, G. Haznedar, D. Scarano, et al., *Carbon*, 2013, **62**, 270–277.
- 22 Y. Wang, Y. Shao, D. W. Matson, et al., *ACS Nano*, 2010, **4**, 1790.
- 23 Z. Liu, J. T. Robinson, X. M. Sun, et al., *J. Am. Chem. Soc.*, 2008, **130**, 10876–10877.
- 24 X. L. Zuo, S. J. He, D. Li, et al., *Langmuir*, 2010, **26**, 1936.
- 25 P. H. G. Kumar and M. A. Xavio, *Procedia Eng.*, 2014, **97**, 1033–1040.

- 26 S. Bai and X. Shen, *RSC Adv.*, 2012, 2, 64–91.
- 27 J. Matos, J. Laine and J. M. Herrmann, *Appl. Catal., B*, 1998, 18, 281–291.
- 28 A. Castellanos-Gomez, M. Poot, G. A. Steele, et al., *Adv. Mater.*, 2012, 24, 772–775.
- 29 A. P. S. Gaur, S. Sahoo, M. Ahmadi, et al., *J. Phys. Chem. C*, 2013, 117, 26262–26268.
- 30 M. Ruinat de Brimont, C. Dupont, A. Daudin, et al., *J. Catal.*, 2012, 286, 153–164.
- 31 N. Singh, G. Jabbour and U. Schwingenschlögl, *Eur. Phys. J. B*, 2012, 85, 392–395.
- 32 X. Zhou, Z. Wang, W. Chen, et al., *J. Power Source*, 2014, 251, 264–268.
- 33 N. Lingappan and D. J. Kang, *Electrochim. Acta*, 2016, 193, 128–136.
- 34 C. Zhai, M. Zhu, D. Bin, et al., *J. Power Sources*, 2015, 275, 483–488.
- 35 Y. Jing, E. O. Ortiz-Quiles, C. R. R. Cabrera, et al., *Electrochim. Acta*, 2014, 147, 392–400.
- 36 J. Liu, Z. Zeng, X. Cao, et al., *Small*, 2012, 8, 3517–3522.
- 37 G. Du, Z. Guo, S. Wang, et al., *Chem. Commun.*, 2010, 46, 1106–1108.
- 38 A. A. Jeffery, C. N. Ethravathi and M. Rajamathi, *J. Phys. Chem. C*, 2014, 118, 1386–1396.
- 39 L. A. King, W. Zhao, M. Chhowalla, et al., *J. Mater. Chem. A*, 2013, 1, 8935–8941.
- 40 Y. Li, Y. Li, C. M. Araujo, et al., *Catal. Sci. Technol.*, 2013, 3, 2214–2220.
- 41 G. Eda, H. Yamaguchi, D. Voiry, et al., *Nano Lett.*, 2011, 11, 5111–5116.
- 42 Y. Chen, H. Ge, L. Wei, et al., *Catal. Sci. Technol.*, 2013, 3, 1712–1717.
- 43 L. K. Pan, X. J. Liu, Z. Sun, et al., *J. Mater. Chem. A*, 2013, 1, 8299–8326.
- 44 C. M. Hansen, *Hansen Solubility Parameters, A User's Handbook*, CRC Press, Taylor and Francis Group, 2000.
- 45 J. N. Coleman, M. Lotya, A. O'Neill, et al., *Science*, 2011, 331, 568–571.
- 46 G. Cunningham, M. Lotya, C. S. Cucinotta, et al., *ACS Nano*, 2012, 6, 3468–3480.
- 47 L. Muscuso, S. Cravanzola, F. Cesano, et al., *J. Phys. Chem. C*, 2015, 119, 3791–3801.
- 48 G. R. Bhimanapati, Z. Lin, V. Meunier, et al., *ACS Nano*, 2015, 9, 11509–11539.
- 49 A. Allain, J. Kang, K. Banerjee, et al., *Nat. Mater.*, 2015, 14, 1195–1205.
- 50 W. Hu, T. Wang, R. Zhang, et al., *J. Mater. Chem. C*, 2016, 4, 1776–1781.
- 51 P. Ganesh, J. Kim, C. Park, et al., *J. Chem. Theory Comput.*, 2014, 10, 5318–5323.
- 52 S. H. Huh, *Physics and Applications of Graphene - Experiments*, ed. S. Mikhailov, 2011.
- 53 K.-G. Zhou, N.-N. Mao, H.-X. Wang, et al., *Angew. Chem., Int. Ed.*, 2011, 50, 10839–10842.
- 54 T. Wu, X. Wang, H. Qiu, et al., *J. Mater. Chem.*, 2012, 22, 4772–4779.
- 55 P. Cui, J. Lee, E. Hwang, et al., *Chem. Commun.*, 2011, 47, 12370–12372.
- 56 Z. Q. Li, C. J. Lu, Z. P. Xia, et al., *Carbon*, 2007, 45, 1686–1695.
- 57 P. V. Kumar, N. M. Bardhan, S. Tongay, et al., *Nat. Chem.*, 2014, 6, 151–158.
- 58 T. Kaplas and P. Kuzhir, *Nanoscale Res. Lett.*, 2016, 11, 1–6.
- 59 A. Splendiani, L. Sun, Y. Zhang, et al., *Nano Lett.*, 2010, 10, 1271–1275.
- 60 U. Bhanu, M. R. Islam, L. Tetard, et al., *Sci. Rep.*, 2014, 4, 5575.
- 61 K. F. Mak, K. He, J. Shan, et al., *Nat. Nanotechnol.*, 2012, 7, 494–498.
- 62 N. Kang, H. P. Paudel, M. N. Leuenberger, et al., *J. Phys. Chem. C*, 2014, 118, 21258–21263.
- 63 J. I. Peterson, R. V. Fitzgerald and D. K. Buckhold, *Anal. Chem.*, 1984, 56, 62–67.
- 64 M. R. Laskar, L. Ma, S. Kannapan, et al., *Appl. Phys. Lett.*, 2013, 102, 252108.
- 65 J. P. Wilcoxon, P. P. Newcomer and G. A. Samara, *J. Appl. Phys.*, 1997, 81, 7934–7944.
- 66 A. Lazzarini, A. Piovano, R. Pellegrini, et al., *Catal. Sci. Technol.*, 2016, DOI: 10.1039/c6cy000159a.
- 67 T. Wu, X. Wang, H. Qiu, et al., *J. Mater. Chem.*, 2012, 22, 4772–4779.
- 68 G. Eda, C. Mattevi, H. Yamaguchi, et al., *J. Phys. Chem. C*, 2009, 113, 15768–15771.
- 69 F. Cesano, M. M. Rahman, S. Bertarione, et al., *Carbon*, 2012, 50, 2047–2051.
- 70 S. Cravanzola, L. Muscuso, F. Cesano, et al., *Langmuir*, 2015, 31, 5469–5478.
- 71 M. J. Uddin, F. Cesano, F. Bonino, et al., *J. Photochem. Photobiol., A*, 2007, 189, 286–294.
- 72 Q. Xiang, J. Yu and M. Jaroniec, *Chem. Soc. Rev.*, 2012, 41, 782–796.
- 73 G. Jiang, Z. Lin, C. Chen, et al., *Carbon*, 2011, 49, 2693–2701.
- 74 J. Li, X. Liu, L. Pan, et al., *RSC Adv.*, 2014, 4, 9647.

Designing rGO/MoS₂ hybrid nanostructures for photocatalytic applications

Sara Cravanzola, Federico Cesano*, Giuliana Magnacca, Adriano Zecchina, Domenica Scarano

Department of Chemistry, NIS (Nanostructured Interfaces and Surfaces) Interdepartmental Centre and INSTM Centro di Riferimento, University of Torino, Via P. Giuria, 7, 10125 Torino, Italy.

*E-mail: federico.cesano@unito.it

Electronic Supplementary Information (ESI)

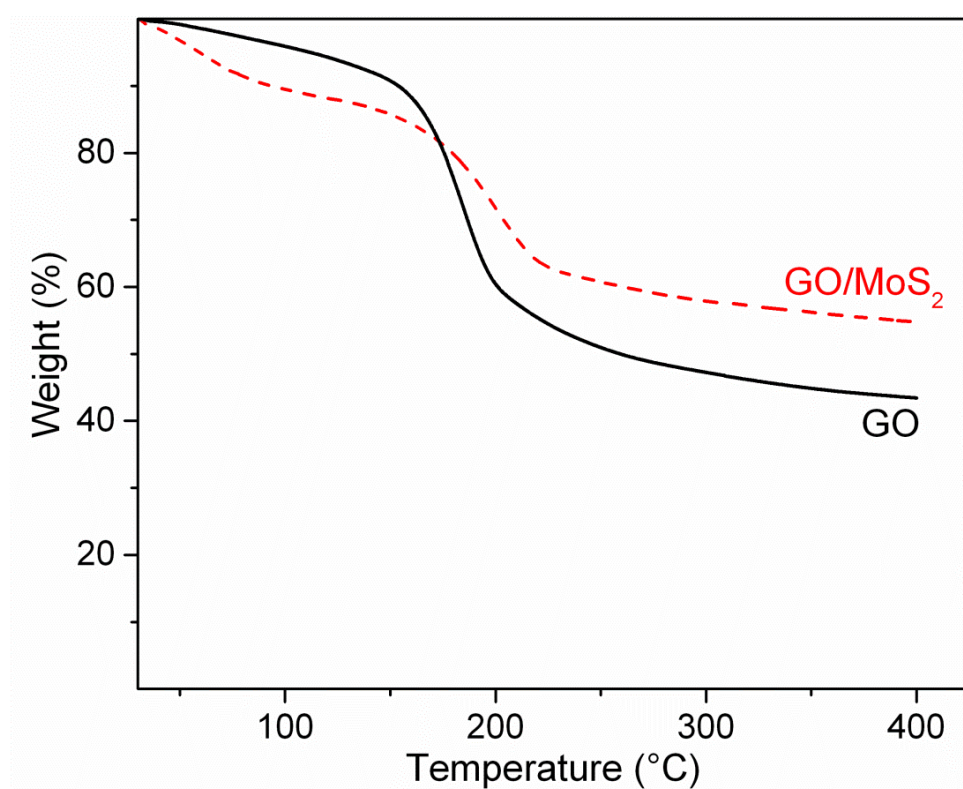


Fig. S1. TGA curve of GO and of GO/MoS₂ under N₂ atmosphere, 5°C/min up to 400°C.

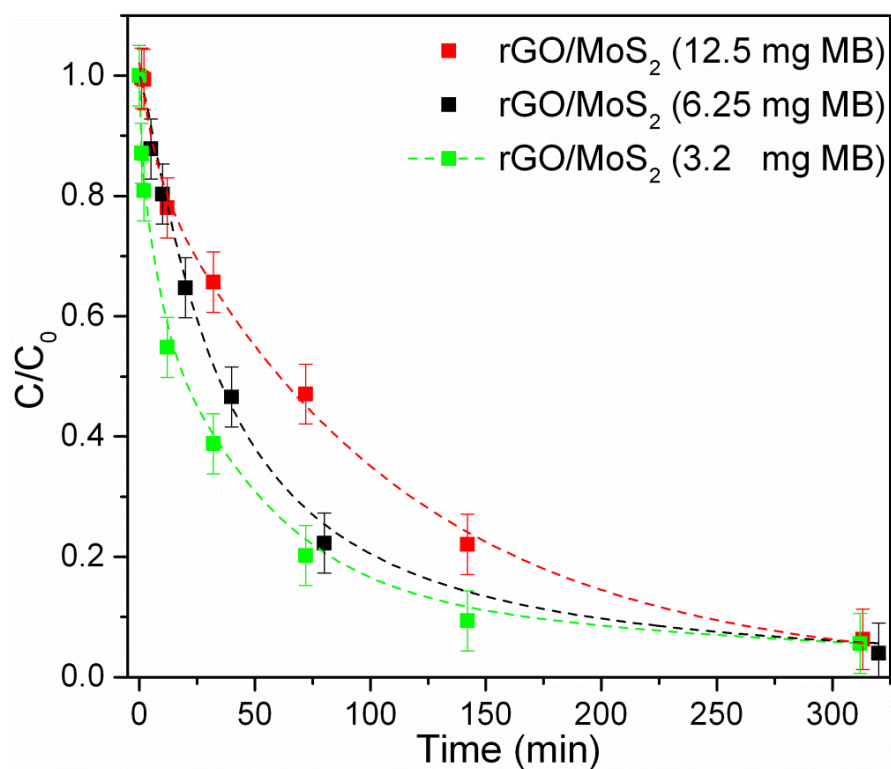


Fig. S2. Time dependence upon light exposure of MB adsorbed on rGO/MoS₂ for the three different initial concentrations of MB: 12.5 mgL⁻¹, 6.25 mgL⁻¹ and 3.2 mgL⁻¹.